Dynamic Element Matching Techniques for Static and Dynamic Errors in Continuous-Time Multi-Bit $\Delta\Sigma$ Modulators

Arindam Sanyal, *Student Member, IEEE*, and Nan Sun, *Member, IEEE*

***Abstract*—This paper presents techniques to address static and dynamic errors in high performance continuous-time (CT), $\Delta\Sigma$ modulators. The inter-symbol interference (ISI) model is presented and existing ISI reduction techniques are reviewed. A novel technique has been presented which can high-pass shape both static mismatch and ISI error of each element of a multi-bit DAC while decorrelating the instantaneous number of transitions from the input signal. The proposed technique can easily be extended to higher order shaping for both static mismatch and ISI errors. Simulation results show that the proposed technique can improve DAC linearity significantly in presence of both static mismatch and ISI error.**

***Index Terms*—Analog-to-digital converter (ADC), device mismatch, digital-to-analog converter (DAC), dynamic element matching, dynamic error, inter-symbol interference (ISI), mismatch shaping, thermometer coding, $\Delta\Sigma$ modulator.**

I. Introduction

CONTINUOUS-TIME (CT) $\Delta\Sigma$ modulators have gained more popularity than discrete-time (DT) $\Delta\Sigma$ modulators in recent times. This is because CT $\Delta\Sigma$ modulators can operate at a higher sampling frequency (f_s) than DT $\Delta\Sigma$ modulators and/or consume less power. In both CT and DT $\Delta\Sigma$ modulators, multi-bit modulators are more popular than their single-bit counterparts because they can achieve higher stability while ensuring higher signal-to-quantization noise ratio (SQNR) due to more aggressive noise shaping. By using a multi-bit modulator, out-of-band noise (OBN) can be lowered for reduced jitter sensitivity. A lower OBN also relaxes the linearity and slew rate requirement for the first-stage integrator in an analog-to-digital converter (ADC) or the reconstruction filter in a digital-to-analog converter (DAC). However, multi-bit modulators suffer from nonlinearity due to static element mismatch which degrades their performance. There are two popular ways to handle element mismatches (1) analog/digital calibration, and (2) dynamic element matching (DEM). Calibration techniques [1]–[3] usually require some apriori knowledge of the device mismatch and very precise measurement of the mismatch error. By contrast, DEM techniques do not need any information about device mismatch. In addition, DEM techniques are purely digital and thus scaling friendly. They consume low power and area at advanced technology nodes.

There are several DEM techniques that have been reported in literature. The technique in [4] whitens element mismatch by randomly selecting the elements. The data weighted averaging (DWA) technique [5]–[7] can first-order shape element mismatch by barrel shifting the element selection pattern. Higher order mismatch shaping can be done by more advanced DEM algorithms [8]–[12].

In addition to static mismatch, CT $\Delta\Sigma$ modulators also suffer from inter-symbol interference (ISI) which does not affect DT $\Delta\Sigma$ modulators. ISI is a dynamic error which shows up during transition of DAC elements and is present in both single-bit and multi-bit CT modulators. Different from static mismatch, ISI error increases with sampling frequency. Hence, it is more problematic for high speed CT $\Delta\Sigma$ modulators. ISI can be caused by asymmetric on and off switching, clock skew and parasitic memory effects.

An analog approach to reduce ISI error is to use return-to-zero (RZ) coding. However, it increases sensitivity to clock jitter compared to non-return-to-zero (NRZ) coding. RZ coding also reduces the output signal amplitude for the same total DAC power, and introduces large discontinuities in the output waveform. This in turn increases the linearity and slew rate requirements of the output filter.

Researchers have attempted to reduce ISI error by reducing the asymmetry between on and off switching in the DAC. The technique in [13] controls the on/off delay by adjusting the threshold of the switching transistors. The work of [14] shows that differential DACs can reduce ISI by using relatively fast and identical transistors. The work of [15] reports that they can reduce ISI error by using only native NMOS transistors to build a current steering DAC. These techniques rely on the ability to ensure good matching between the switches.

The techniques of [16]–[18] use pulse-width modulation (PWM) to force the switching rate of the DAC to be dominated by the PWM carrier frequency and thus be independent of the input. Thus, use of PWM can prove to be very effective against ISI error. PWM is usually followed by a finite-impulse-re-

Manuscript received April 29, 2015; revised July 30, 2015; accepted September 29, 2015. Date of publication December 04, 2015; date of current version December 23, 2015. This work was supported in part by the National Science Foundation ECCS-1254459. This paper was recommended by Guest Editor K.-P. Pun.

The authors are with The Department of Electrical and Computer Engineering, University of Texas at Austin, TX 78712 USA (e-mail: arindam3110@utexas.edu; nansun@mail.utexas.edu).

Color versions of one or more of the figures in this paper are available online at http://ieeexplore.ieee.org.

Digital Object Identifier 10.1109/JETCAS.2015.2502160

sponse (FIR) DAC which places notches at the PWM carrier frequency and its harmonics to reduce nonlinearity associated with PWM. Mismatches in the FIR DAC will shift the placement of the notches and will increase the out-of-band noise and distortion but will not affect the in-band noise. Also, the PWM technique itself does not increase the in-band quantization noise. However, in this approach the FIR DAC requires a clock frequency which is much higher than the sampling frequency f_s. It may not be possible to generate such a high clock rate for many applications specially when f_s itself is quite high.

In contrast to the PWM approach, DEM algorithms do not require clock frequencies higher than the sampling frequency. However, most existing mismatch shaping DEM algorithms are designed for DT $\Delta\Sigma$ modulators and cannot mitigate ISI error. This is because DEM algorithms increase the DAC element switching rate to shape static mismatch. However, increased switching activity deteriorates ISI error. DWA is the worst when it comes to ISI error, because it has the highest element switching activity among the traditional DEM algorithms. Higher order DEMs perform better than DWA because they can shape away the static mismatch with lower element switching activity than DWA. Nonetheless, traditional DEM algorithms are still not suitable to address both static mismatch and ISI error simultaneously.

From a purely ISI point of view, thermometer coding is the best technique as it has the minimum element switching rate. Also, for sufficiently large out-of-band noise gain and/or high over-sampling ratio (OSR), the switching activity of thermometer coding will be dominated by quantization noise. Hence, thermometer coding will show low ISI induced distortion as the element transition density has low dependence on input. However, as the OSR is reduced, thermometer coding will show higher ISI induced distortion as the element transition density will have more dependence on input. Also, thermometer coding cannot handle static mismatch. To address this issue, modified thermometer coding schemes [19]–[21] have been developed which use intrinsic quantization noise to randomize the element selection pattern. The limitation of this approach is that the static mismatch reduction is not as effective as other DEM techniques, since the static mismatch is not high-pass shaped. The modified thermometer technique of [22] achieves high-pass shaping of static mismatch in addition to minimizing ISI error.

The modified thermometer coding techniques rely on minimizing the number of transitions to reduce ISI error. The modified mismatch shaping (MMS) technique [23] presents another way of reducing ISI error. It made an important observation that ISI error can be reduced significantly by reducing the correlation between the input and DAC element transition sequence. This way, a large part of the ISI error is simply turned to an offset and does not degrade output linearity. Accordingly, the MMS technique tries to ensure that the DAC maintains the total number of up and down transitions every cycle relatively constant. Despite its clear advancement over prior works, MMS technique has some limitations. It assumes both up and down transitions contribute equal ISI error which does not cover all possible ISI scenarios. Also, it requires good matching between ISI errors of individual DAC elements.

The ISI shaping technique of [24] represents a major improvement over the MMS technique. A general model for ISI error is developed in [24] and it has been shown that nonlinearity due to ISI can be attributed completely to only one of the four possible transitions $(0 \rightarrow 0, 0 \rightarrow 1, 1 \rightarrow 0, 1 \rightarrow 1)$. Thus, by ensuring that the long term average of only the up transition $(0 \rightarrow 1)$ remains constant, the ISI error can be high-pass shaped. Building on the ISI shaping technique of [24], our prior work [25] reduces the in-band ISI error further by monitoring both the up and down transitions. However, the techniques of both [24] and [25] suffer from ISI induced distortion at large signal amplitudes. This is because at large signal amplitudes, the instantaneous number of DAC element transitions is still correlated with the input signal even though the long term average of the transitions is constant. To address this issue, the technique reported in [26] ensures that the number of transitions of the DAC element is uncorrelated with the input signal at every cycle. Thus, it can achieve a very good decorrelation between instantaneous transition density and the input signal. Yet it has a limitation that even though the overall ISI error is high-pass shaped, ISI error for each individual DAC element is not shaped. In presence of mismatch between ISI errors of the different elements, the in-band noise can be increased. Note that [24], [25] do not have this limitation.

In this paper, we propose a novel DEM technique to address this limitation. The proposed technique monitors the up transition density for each element in the DAC, and selects the element pattern in such a way that the long term up transition density of each element is identical. Thus, the ISI error for each element is high-pass shaped. This is done in addition to high-pass shaping the static mismatch and decorrelating the instantaneous transition density from the input. The key contributions of this paper are

1) A thorough review of existing DEM based ISI reduction techniques is provided.
2) A novel DEM which can high-pass shape static mismatch as well ISI error for individual DAC element is presented.

The paper is organized as follows. Section II presents the ISI error model. Section III presents a review of prior works on ISI reduction. Section IV presents the proposed DEM. Section V presents simulation results and the conclusion is brought up in Section VI.

II. ISI Model

In this section, the ISI model is presented for a $\Delta\Sigma$ DAC. However, the model is equally valid for a $\Delta\Sigma$ ADC as the effects of ISI error is same for both $\Delta\Sigma$ ADC and DAC. The general architecture of a $\Delta\Sigma$ DAC is shown in Fig. 1. Let us use $d_i[n]$ to represent the single-bit digital input for the i-th unit element DAC in a multi-bit DAC.

The vector-quantizer (VQ) based structure [8] of Fig. 2, is a well known way to implement the DEM logic in Fig. 1.

The discrete time representation of the unit element DAC output $v_i[n]$ in the presence of mismatch and ISI errors can be written as

$$v_i[n] = (1 + \delta_i)d_i[n] + \mathrm{ISI}_i[n] \tag{1}$$

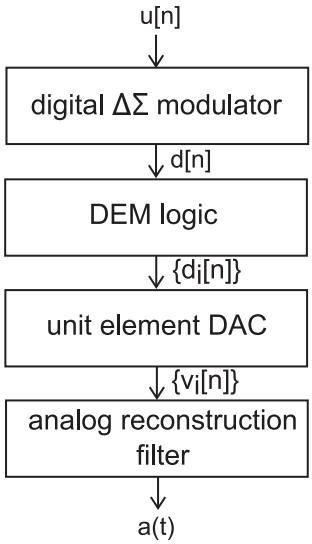

Fig. 1. General architecture of a ΔΣ DAC.

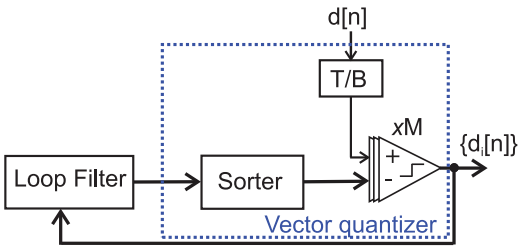

Fig. 2. Standard vector quantizer diagram.

where δ_i represents the static mismatch and $\text{ISI}_i[n]$ represents the dynamic ISI error during transition from $d_i[n-1]$ to $d_i[n]$.

The ISI error model is shown in Fig. 3. For the i-th element in the DAC, the time integral of the ISI error pulses are denoted by e_{00i}, e_{01i}, e_{10i} and e_{11i} corresponding to the four transitions $(0 \to 0, 0 \to 1, 1 \to 0, 1 \to 1)$. The ISI error can then be written as

$$\begin{aligned}\text{ISI}_i[n] &= e_{00i}(1-d_i[n-1])(1-d_i[n]) \\ &\quad + e_{10i}d_i[n-1](1-d_i[n]) + e_{11i}d_i[n-1]d_i[n] \\ &\quad + e_{01i}(1-d_i[n-1])d_i[n] \\ &= e_{00i} + (e_{10i}-e_{00i})d_i[n-1] + (e_{11i}-e_{10i})d_i[n] \\ &\quad + (e_{10i}+e_{01i}-e_{11i}-e_{00i})(1-d_i[n-1])d_i[n] \\ &\equiv \alpha_i + \gamma_i d_i[n-1] + \beta_i d_i[n] + \epsilon_i \Gamma_i[n] \end{aligned} \tag{2}$$

where α_i, β_i, γ_i and ϵ_i are the normalized ISI error coefficients and given by $\alpha_i = e_{00i}$, $\beta_i = (e_{11i}-e_{10i})$, $\gamma_i = (e_{10i}-e_{00i})$ and $\epsilon_i = (e_{10i}+e_{01i}-e_{00i}-e_{11i})$. The coefficients α_i, β_i, γ_i and ϵ_i are constants which depend on the circuit implementation but do not depend on $d[n]$. Their values increase with increase in f_s. $\Gamma_i[n]$ represents the up-transition sequence given by $(1-d_i[n-1])d_i[n]$.

The first three terms of (2) represent a 2-tap filtering of $d_i[n]$ and constitute the linear part of ISI error, while the fourth term introduces nonlinearity. As has been shown in [24], [25], the nonlinearity can be also associated with any one of the other 3 transitions $(0 \to 0, 1 \to 0, 1 \to 1)$. It should be noted that in presence of static mismatch, β_i and γ_i will introduce distortion in the DAC output.

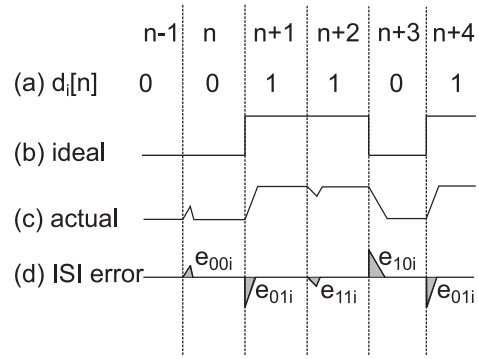

Fig. 3. (a) 1-bit digital sequence (b) ideal DAC output (c) DAC output with ISI error (d) ISI error.

Plugging (2) into (1), we get

$$v_i[n] = \alpha_i + (1+\delta_i+\beta_i)d_i[n] + \gamma_i d_i[n-1] + \epsilon_i \Gamma_i[n] \tag{3}$$

Assuming the law of superposition holds, the output of M-element DAC can be written as

$$\begin{aligned} v[n] &= \sum_{i=1}^{M} v_i[n] \\ &= d[n] + \sum_{i=1}^{M}\alpha_i + \sum_{i=1}^{M}(\delta_i+\beta_i)d_i[n] \\ &\quad + \sum_{i=1}^{M}\gamma_i d_i[n-1] + \sum_{i=1}^{M}\epsilon_i\Gamma_i[n] \end{aligned} \tag{4}$$

From (4), it can be seen that distortion in $v[n]$ can come from static mismatch or from nonlinear ISI error which is contributed by $\Gamma_i[n]$.

$$\begin{aligned} \sum_{i=1}^{M}\epsilon_i\Gamma_i[n] &= \sum_{i=1}^{M}\epsilon(1+\epsilon_{ri})\Gamma_i[n] \\ &= \epsilon\left(\sum_{i=1}^{M}\Gamma_i[n] + \sum_{i=1}^{M}\epsilon_{ri}\Gamma_i[n]\right) \\ &= \epsilon\left(\Gamma[n] + \sum_{i=1}^{M}\epsilon_{ri}\Gamma_i[n]\right) \end{aligned} \tag{5}$$

where ϵ_{ri} represents the relative mismatch in ϵ_i among the different DAC elements. This model shows that for the DAC output $v[n]$ to be free of distortions, we have to ensure no distortion in $d_i[n]$ and $\Gamma_i[n]$.

Even though the ISI model assumes that law of superposition holds, in practice this maybe a simplification of the real scenario. This is because ISI error of one DAC element may influence ISI error of another DAC element. However, even with this limitation, the model is still useful as it provides key insights into ISI error and ways to reduce it.

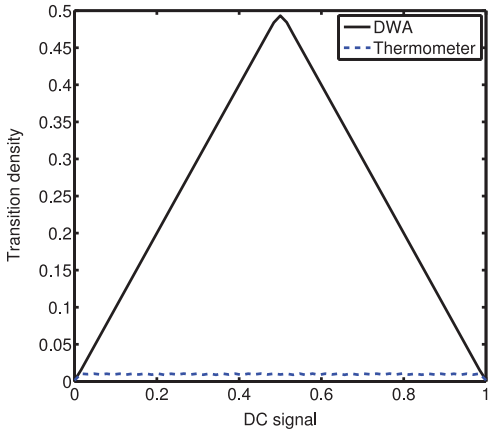

Fig. 4. Simulated transition density versus signal amplitude for DWA and thermometer coding.

III. Review of Prior DEM Techniques

A. Modified Thermometer Coding Techniques

DWA has been a much used technique to address static mismatch. DWA high-pass shapes static mismatch error and thus reduces its contribution to the in-band noise. Thus, DWA is a very good technique for discrete time $\Delta\Sigma$ modulators where static mismatch is the main source of error. The strength of DWA is that it has the highest element switching activity and thus can scramble the element selection very effectively. However, it follows from the ISI model that a high element switching rate increases the ISI error. Thus, use of DWA is not beneficial for CT $\Delta\Sigma$ modulators where ISI is a major concern. From ISI perspective, thermometer coding is a very good candidate as it minimizes the element switching rate. Further, since the switching rate in thermometer coding is usually determined by the intrinsic quantization noise for high OSR and/or large out-of-band NTF gain scenarios, the correlation between DAC switching sequence and the input signal is also very low. Thus, thermometer coding does not show ISI induced distortion. This makes thermometer coding much more attractive than DWA for CT $\Delta\Sigma$ modulators in presence of ISI error. Fig. 4 shows the simulated transition density versus dc signal for both DWA and thermometer coding. A 32 element second-order $\Delta\Sigma$ DAC with an out-of-band NTF gain of 2 was used for the simulation. The input dc signal's amplitude was swept to get the transition density variation. It can be seen that thermometer coding has a very low transition density with very low correlation with the input. On the other hand, DWA has a large transition density and the folding of the transition density around the middle of the signal range contributes to the large nonlinearity in $\Gamma[n]$ for DWA. Note that the transition density of DWA in Fig. 4 is slightly lower than the theoretical maximum of 0.5 due to the presence of random noise in the simulation which reflects real operating conditions.

Even though thermometer coding has a very low switching activity, it still cannot handle static mismatch error. This has prompted researchers to modify the basic thermometer coding and build on it to address both static mismatch and ISI error. The randomized thermometer coding (RTC) technique of [19] tries to keep a low element switching activity by using a modified thermometer coding. To randomize the static mismatch, the starting element of thermometer coding is changed randomly after a certain number of input samples. Thus, it tries to balance both static mismatch and ISI error. However, the element switching activity of [19] is still more than the basic thermometer coding as it allows more transitions to randomize element mismatch. The random swapping thermometer coding (RSTC) algorithm [20] tries to address this limitation in the RTC technique by randomizing the element selection pattern while maintaining the same number of transitions as thermometer coding. RSTC technique does this by randomizing the start/stop position of the element selection while ensuring maximum overlap in the element selection pattern. However, it does not fully whiten static mismatch leading to increased noise floor. The technique proposed in [21] achieves a better randomization of element mismatch than RSTC while still having the same minimum switching activity as thermometer coding. The operation of the technique in [21] can be described as

1) If $d[n] = d[n-1]$, no change in the element selection pattern.
2) If $d[n] > d[n-1]$, turn on $(d[n] - d[n-1])$ unselected elements randomly.
3) If $d[n] < d[n-1]$, turn off $(d[n-1] - d[n])$ selected elements randomly.

An advantage of the technique of [21] over RSTC is that the DAC element usage for [21] is more distributed than RSTC. Thus, a DAC using the technique in [21] has better protection from gradient errors, and thus better performance than RSTC.

While the techniques of [19]–[21] all randomize static mismatch and ISI error simultaneously, they share the limitation of not high-pass shaping static mismatch error. The work of [22] makes a significant contribution by introducing the capability to high-pass shape static mismatch while maintaining DAC switching activity similar to thermometer coding. The work of [22] builds directly on the work of [21]. Fig. 5 shows the architecture of the DEM proposed in [22]. The structure is similar to the conventional VQ structure. The only difference is the insertion of an additional feedback loop with a gain G.

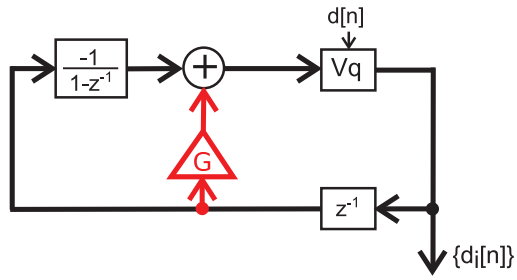

Fig. 5. Architecture of the DEM in [22].

The operation of the technique of [22] can be divided into 3 cases.

1) If $d[n] = d[n-1]$, no change in the element selection pattern.
2) If $d[n] > d[n-1]$, turn on $(d[n] - d[n-1])$ unselected elements that have been least frequently used.
3) If $d[n] < d[n-1]$, turn off $(d[n-1] - d[n])$ selected elements that have been most frequently used.

TABLE I
VARIATION OF SNDR WITH G

	G					
SNDR(dB)	0	0.1	1	10	100	1000
0.1% static, 0.1% ISI	66	73.5	77.4	72.4	71.4	71.4
0.5% static, 0.1% ISI	67.4	74.9	78.8	80.8	79.9	79.9
0.1% static, 0.5% ISI	53.3	60.7	64.7	72.1	71.7	71.7
0.3% static	103.1	99.7	95	73.8	72.9	72.9
0.3% ISI	58.5	66	69.9	77.7	77.5	77.5

TABLE II
VARIATION OF UP-TRANSITION DENSITY WITH G

	G					
	0	0.1	1	10	100	1000
up-transition density	0.28	0.19	0.13	0.05	0.05	0.05

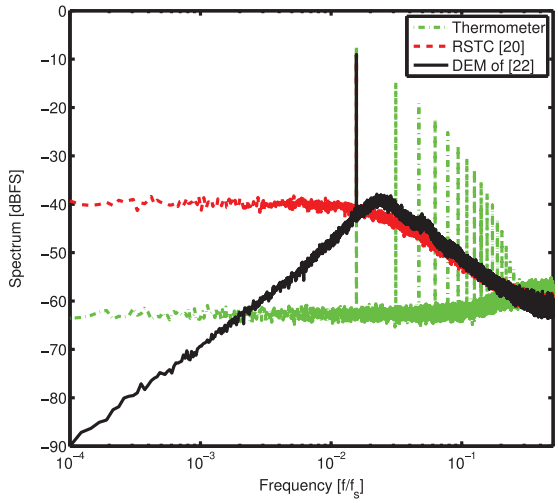

Fig. 6. Spectra of $\{d_i[n]\}$ for thermometer, RSTC [20] and DEM of [22].

This way, the transition rate of the DEM in [22] is as low as that of thermometer coding, while still shaping static mismatch in the DAC. There is a design trade-off in selection of the feedback loop gain, G. If $G = 0$, the DEM is equivalent to a first order VQ, or DWA, which only shapes the static mismatch, but has a large ISI error. If G is high, the element transition rate starts approaching that of pure thermometer coding, thus having low ISI error but not shaping the static mismatch. This trade-off can also be seen from Table I. The simulations for Table I are performed with a 15-element third-order $\Delta\Sigma$ DAC with a maximum out-of-band noise transfer function (NTF) gain of 6 and a -3 dBFS input.

As can be seen from Table I, a lower value of G increases the signal-to-noise-and-distortion ratio (SNDR) if static mismatch is the dominant source of DAC non-ideality. If ISI error dominates, SNDR increases with G. At very high G, the technique of [22] becomes the same as basic thermometer coding, and no further improvement is seen in SNDR for ISI error limited DAC.

Table II shows the variation of up transition density with G. The simulation conditions used to generate Table II are the same as for Table I. It can be seen from Table II that at very high G, the up-transition density does not change with G. This is because the transition density of the modified thermometer coding technique of [22] becomes the same as that of basic thermometer coding at very high G.

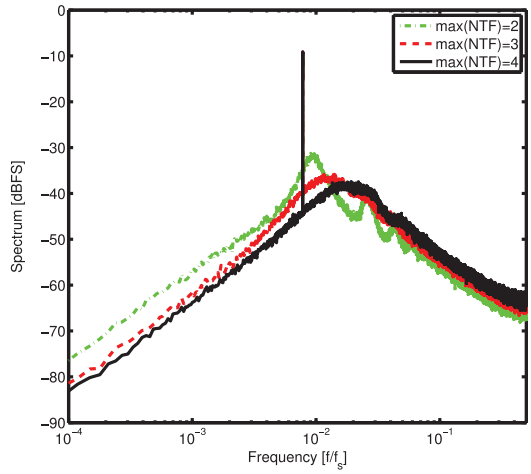

Fig. 7. Spectra of $\{d_i[n]\}$ for the DEM of [22] for different maximum NTF gains.

To verify the efficacy of the static mismatch shaping performance of the modified thermometer coding of [22] and compare it against basic thermometer coding and RSTC technique [20], the spectra of the selection pattern $\{d_i[n]\}$ for the three techniques are plotted in Fig. 6. Note that the spectrum of $\{d_i[n]\}$ refers to the spectrum of $d_i[n]$ averaged over all the elements. A 32-element fifth-order $\Delta\Sigma$ DAC with a maximum out-of-band NTF gain of 6 was used for the simulation. An input of -3 dBFS and frequency of $f_s/64$ was used. G was set to 10 for the simulation. The basic thermometer coding has a lot of tones because its element selection pattern is highly correlated with the input $d[n]$. Both [20] and [22] do not show harmonics due to randomization of the element selection pattern. The technique of [22] also shapes the mismatch error and has a much lower in-band error component than the RSTC technique of [20].

To get an understanding of the noise-shaping characteristic of the DEM in [22], let us model the VQ by a linear gain K and a quantization error q.

$$\begin{aligned} d_i &= \left(\frac{z^{-1}}{1-z^{-1}}(d-d_i) + Gz^{-1}d_i\right)K + q \\ \Longrightarrow d_i &= \left(\frac{z^{-1}K}{1+(K-1-GK)z^{-1}+GKz^{-2}}\right)d \\ &\quad + \left(\frac{1-z^{-1}}{1+(K-1-GK)z^{-1}+GKz^{-2}}\right)q \\ &\equiv H_1(z)d + H_2(z)q \end{aligned} \tag{6}$$

It can be seen from (6) that $H_2(z)$ has a first-order shaping at low frequencies and a low gain at high frequencies. The gain of $H_2(z)$ at high frequencies $(z = -1)$ is $2/(2-K+2GK) \approx 1/GK$. For high values of G, this gain will be low. This can also be seen from the spectrum in Fig. 6. A low gain at high frequency indicates a low transition rate.

It should be pointed here that the mismatch shaping performance of the technique in [22] depends on the randomization of DAC element selection. The randomization depends heavily on the quantization noise. Thus, it is expected that increase in maximum out-of-band NTF gain will improve the mismatch shaping performance of the DEM. This can also be seen from Fig. 7 which shows that for higher out-of-band NTF gain, the DEM of [22] will achieve a lower in-band noise when only static mismatch is present.

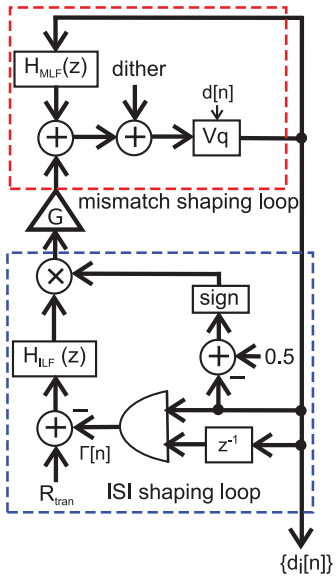

Fig. 8. Architecture of ISI shaping technique of [24].

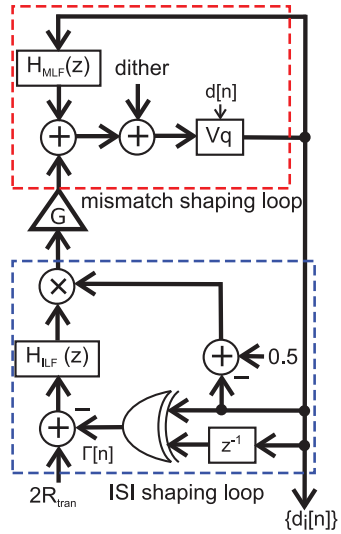

Fig. 9. Architecture of ISI shaping technique of [25].

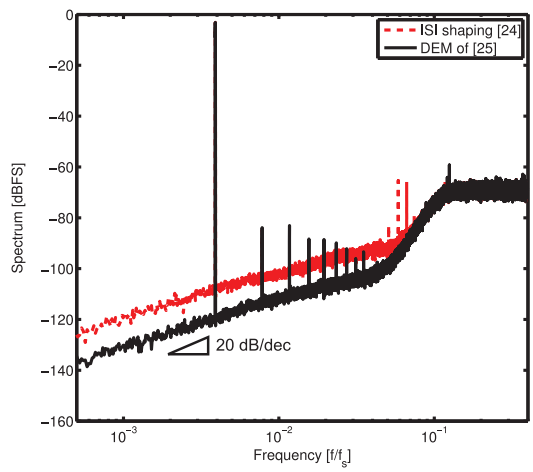

Fig. 10. DAC output spectra comparison between ISI shaping technique of [24] and DEM of [25].

B. MMS Algorithm

The MMS algorithm [23] presents a change of perspective in addressing ISI error. Different from modified thermometer coding techniques which rely on minimizing element transition to reduce ISI error, MMS algorithm tries to ensure that the total number of transitions is independent of $d[n]$. Making the total number of transitions independent of $d[n]$ can turn ISI error to just an offset and thus significantly improve DAC linearity. However, the MMS algorithm has the following limitations

1) It assumes that all the elements have the same values for e_{00i}, e_{01i}, e_{10i} and e_{11i}.
2) It assumes that $e_{01i} = e_{10i}$.

Inspite of these limitations, MMS algorithm represents a major advancement in the field of ISI reduction. Further, by achieving decorrelation of the total number of transitions and $d[n]$ over a large range of $d[n]$, it reduces ISI induced distortion to a great extent.

C. ISI Shaping Techniques

Another major advancement came in the form of the ISI shaping technique proposed in [24]. This technique showed that ISI error can be high-pass shaped similar to static mismatch. The technique of [24] achieved simultaneous ISI and mismatch shaping by using two separate loops as shown in Fig. 8.

ISI shaping is done by a $\Delta\Sigma$ loop which monitors the up-transition density $\Gamma_i[n]$ of each DAC element and ensures their long term average is equal to a fixed number $R_{\rm tran}$. By controlling the switching activity of individual DAC elements, the technique of [24] solves the limitations of the MMS technique in that it does not require e_{01i} to be equal to e_{10i} and it does not require ISI errors of each DAC element to match.

The ISI shaping technique of [24] monitors only the up transition and not the down transition. A better ISI shaping can be obtained by taking both the up and down transitions into account. The technique proposed in [25] does this. The improvement in ISI shaping performance can be intuitively understood by recognizing a down transition as an intermediate state between two up transitions. Thus, counting down transition can double the resolution of transition rate count, and hence improve the ISI shaping performance. Since the up transition density is equal to the down transition density, shaping the total transition sequence guarantees that both up as well as down transition sequences are shaped. The architecture monitoring both the transitions is shown in Fig. 9.

Comparison of the ISI shaping techniques of [24] and [25] is shown in Fig. 10 for a -3 dBFS input. First order filter is used for both static mismatch and ISI shaping loops. A 32-element DAC with 1% static mismatch and 3% ISI error is used for the comparison. At an OSR of 16, the technique of [25] shows 4 dB higher SNDR than the ISI shaping technique of [24]. This validates the idea of monitoring both up and down transitions in order to achieve a better ISI shaping performance.

A limitation of both the ISI shaping technique of [24] and the DEM proposed in [25] is the presence of distortion at large signal amplitudes. This is also evident from Fig. 10. The distortion comes from the coupling between ISI and mismatch shaping loops. At large signal amplitudes, this coupling is very

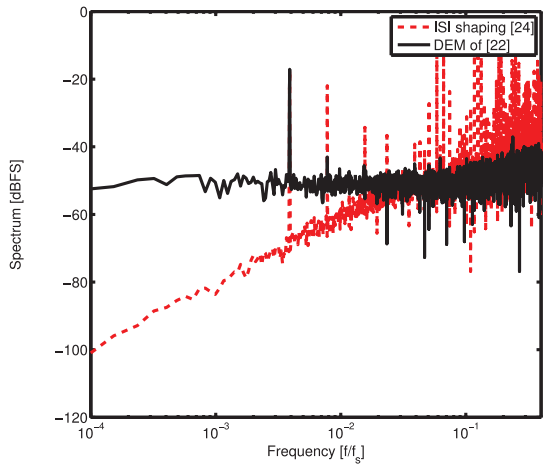

Fig. 11. Spectra of $\Gamma[n]$ for ISI shaping technique [24] and modified thermometer coding of [22].

tight and causes the instantaneous transition density to be dependent on $d[n]$ even though the average transition density is independent of $d[n]$. This is unlike the thermometer based techniques which show excellent decorrelation between instantaneous transition density and $d[n]$. As an example, $\Gamma[n]$ of the ISI shaping technique of [24] and the modified thermometer coding of [22] is shown in Fig. 11. An input amplitude of -3 dBFS was used for the simulation. It can be seen that the technique of [22] shows a much lower second harmonic than ISI shaping technique of [24]. This is due to the decorrelation between $\Gamma[n]$ and $d[n]$ for the modified thermometer coding technique of [22]. Thus, Fig. 11 also highlights the limitation of the ISI shaping technique [24], namely, increased distortion at large signal amplitudes.

D. ISI Shaping With Signal Independent Element Transition Rates

Recently, another technique has been reported in [26] that achieves simultaneous mismatch and ISI shaping while ensuring that the total number of transitions remains independent of $d[n]$. The DEM proposed in [26] achieves ISI shaping by using a $\Delta\Sigma$ modulator to vary the instantaneous number of transitions between three adjacent integers, $L-1$, L and $L+1$. To see how this can be done, let us use $K[n]$ to denote the total number of up and down transitions. The total number of up transitions, $\Gamma[n]$, can then be written as

$$\Gamma[n] = \frac{K[n] + d[n] - d[n-1]}{2} \tag{7}$$

It can be seen from (7) that if $K[n]$ is high-pass shaped and uncorrelated with $d[n]$, ISI error can be shaped without any distortion. $K[n]$ cannot be a constant as $(K[n] + d[n] - d[n-1])$ has to be even, which means that $K[n]$ cannot be completely independent of $d[n]$. Assuming the long term average of $K[n]$ to be L, $K[n]$ can be chosen in the following way to ensure a good decorrelation with $d[n]$:

1) if $(L + d[n] - d[n-1])$ is even, $K[n] = L$.
2) if $(L + d[n] - d[n-1])$ is odd, a $\Delta\Sigma$ modulator sets $K[n]$ to $L-1$ or $L+1$.

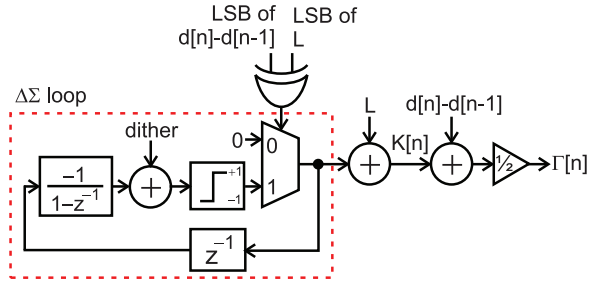

Fig. 12. Circuit block diagram that generates first-order high-pass shaped $K[n]$ and $\Gamma[n]$.

The hardware implementation for generation of $K[n]$ and $\Gamma[n]$ is shown in Fig. 12.

An XOR gate checks parity of $(L + d[n] - d[n-1])$. If it is even, the $\Delta\Sigma$ modulator produces 0 and $K[n]$ is set to L. If $(L+d[n]-d[n-1])$ is odd, $K[n]$ is set to $L\pm1$ according to the output of the modulator. A small and efficient dither is added to remove spurs [27].

Once $K[n]$ is generated, $\Gamma[n]$ is obtained from (7), and the element selection is decided every cycle in the following manner:

1) turn on $\Gamma[n]$ unselected elements that have been least frequently used.
2) keep on $(d[n]-\Gamma[n])$ selected elements that have been least frequently used.

There are requirements on $d[n]$ and $\Gamma[n]$ in order for this algorithm to work. First, $(d[n-1]+\Gamma[n]) \leq M$. If this inequality is violated, step 1) of the algorithm is unrealizable, as the total number of unselected elements is smaller than $\Gamma[n]$. By plugging in (7), this inequality is essentially

$$K[n] \leq (2M - d[n] - d[n-1]) \tag{8}$$

The second requirement is $0 \leq (d[n] - \Gamma[n]) \leq d[n-1]$. If violated, step 2) of the algorithm is invalid because there is insufficient number of elements to keep on. Again plugging in (7), we have

$$(d[n] - d[n-1]) \leq K[n] \leq (d[n] + d[n-1]) \tag{9}$$

These requirements impose constraints on $K[n]$ and the range of $d[n]$. The lower limit for $K[n]$ is $(d[n] - d[n-1])$. In a low-pass $\Delta\Sigma$ modulator with high OSR, the range of $(d[n] - d[n-1])$ is typically set not by the signal but by the noise transfer function. Thus, this limit essentially states that $K[n]$ or L must be equal or greater than the maximum NTF gain. For example, if $\max\{|\mathrm{NTF}(\omega)|\} = 2$, we have $L \geq 2$. Note that for a $\Delta\Sigma$ modulator with low OSR, the maximum value of $(d[n]-d[n-1])$ may be larger than $\max\{|\mathrm{NTF}(\omega)|\}$. In such a case, L needs to be set even larger. Similarly, we can derive the constraints on the range of $d[n]$ from $K[n] \leq (d[n] + d[n-1])$ and $K[n] \leq (2M - d[n] - d[n-1])$. They are equivalent to $K[n] \leq (d[n] + d[n-1]) \leq (2M - K[n])$. Thus, the maximum range for $d[n]$ is smaller than $[0, M]$. For example, if $M = 32$ and $L = 2$, we have $1 \leq d[n] \leq 31$. This constraint is mild as it is only about 1 dB loss in the signal swing. Only if $\max\{|\mathrm{NTF}(\omega)|\}$ is large and M is small simultaneously, the constraint will become tighter. It should be noted here that a moderate value of $\max\{\mathrm{NTF}(\omega)\}$ (e.g., 2 or 3) is

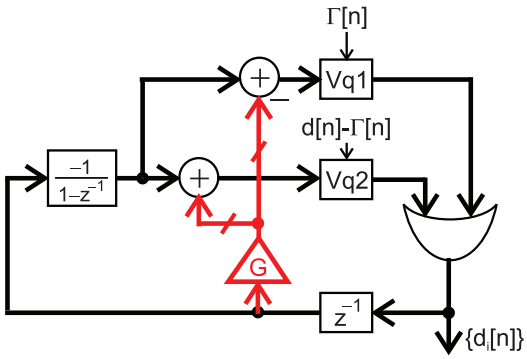

Fig. 13. Implementation of the DEM proposed in [26].

sometimes preferred over a large max $\{\mathrm{NTF}(\omega)\}$. For a $\Delta\Sigma$ ADC, a moderate out-of-band NTF gain results in smaller input swing for the first-stage integrator, thereby improving its linearity and relaxing the slew rate requirement. For a $\Delta\Sigma$ DAC, it relaxes the performance requirement of the analog reconstruction filter. Moreover, a moderate out-of-band gain together with a large M can reduce the amount of out-of-band noise, and thus, reduce the clock jitter sensitivity. In addition to high-speed CT $\Delta\Sigma$ modulators, ISI reduction is also of great importance in high-resolution but low-speed ADCs/DACs, such as those used in high quality audio applications. A large value of M is common in high-quality audio DACs. As an example, the modulator in [24] has a segmented DAC with both the primary and secondary DACs having 32 elements each. In this scenario, the signal swing loss is still small.

It should also be pointed out here that the restriction on the range of $d[n]$ is actually a manifestation of the trade-off between redundancies in element selection and ISI error reduction. There should be adequate redundancy in the DAC for the DEM to select elements so as to reduce ISI error. MMS algorithm [23] has a restriction on the range of $d[n]$ similar to to the DEM proposed in [26]. The ISI shaping technique [24] allows for a larger input swing but suffers from increased distortion.

Hardware implementation of the DEM of [26] is shown in Fig. 13. The modification from the DEM in [22] is the presence of an additional VQ and an additional direct feedback path. A high value of G ensures that the vector quantizer $Vq1$ gives higher priority to elements that are not selected previously and the vector quantizer $Vq2$ gives higher priority to previously selected elements. For efficient hardware implementation, the two summers before $Vq1$ and $Vq2$ can be removed and replaced by a sign bit for inputs to $Vq1$ and $Vq2$. For previously selected elements, the sign bit will be set to '1' for inputs to $Vq2$ and set to '0' for the remaining inputs to $Vq2$. The sign bit for inputs to $Vq1$ are complementary to the inputs to $Vq2$. It should be noted here that G cannot be too small as a very small value of G will violate the condition $d[n] = \sum_{i=1}^{M} d_i[n]$ and result in a high quantization noise. As long as G is sufficiently high, the value of G does not affect the trade-off between static mismatch and ISI error. This can also be seen from the results in Table III. A fifth-order $\Delta\Sigma$ DAC with maximum out-of-band NTF gain of 3 was used for the simulation. A -3 dBFS input at frequency of $f_s/1332$ was used. It can be seen that if ISI is the dominant source of nonlinearity, then the presence of the feedback path with gain G results in a better SNDR than if static mismatch is the dominant source of output nonlinearity. However, change in the value of G does not present any trade-off between static mismatch and ISI error provided that the condition $d[n] = \sum_{i=1}^{M} d_i[n]$ is not violated.

TABLE III
VARIATION OF SNDR WITH G

	G			
SNDR(dB)	5	10	100	1000
1% static, 1% ISI	86.4	86.8	86.8	86.0
5% static, 1% ISI	71.7	73.0	73.1	73.2
1% static, 5% ISI	85.4	85.9	85.7	86.3
3% static	76.6	76.7	76.3	76.9
3% ISI	101.7	101.7	101.5	101.7

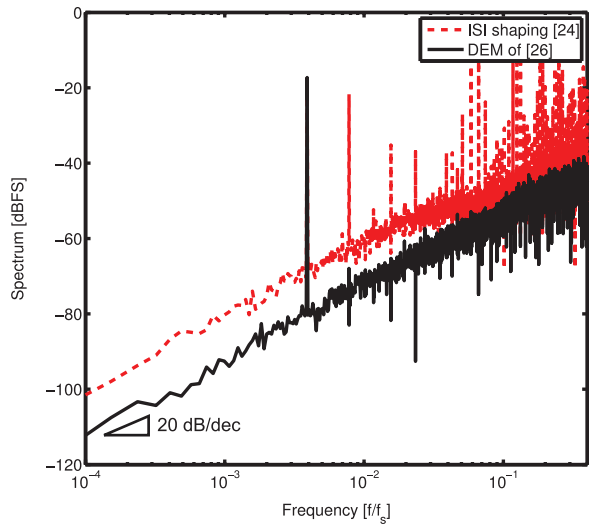

Fig. 14. Spectra of $\Gamma[n]$ for ISI shaping technique of [24] and DEM of [26].

Fig. 14 shows the spectra of up-transition sequence $\Gamma[n]$ for ISI shaping technique of [24] and DEM of [26] for an input amplitude of -3 dBFS. A 32-element DAC with 1% static mismatch error and 1% ISI error was used for the simulation. A maximum out-of-band NTF gain of 3 was used. As can be seen from Fig. 14, the technique in [26] achieves a good decorrelation between $K[n]$ and $d[n]$ and hence, does not show harmonic distortion like the ISI shaping technique of [24].

The technique in [26] monitors only the total number of transitions $K[n]$ as opposed to the ISI shaping technique [24] that monitors the transition of each DAC element. The result is having less hardware complexity at the expense of not shaping the transition sequence for each element even though the overall transition sequence is shaped. This can also be seen from Fig. 15 which shows the spectra of $\Gamma_i[n]$ for ISI shaping technique of [24] and the technique of [26]. The simulation conditions are the same as used for Fig. 14. $\Gamma_i[n]$ for the technique in [26] is not shaped even though $\Gamma[n]$ is shaped. The limitation of not shaping $\Gamma_i[n]$ is an increased noise floor at low frequencies in presence of mismatch in ISI error between the different DAC elements. Note that the spectrum of $\Gamma_i[n]$ shows peaks at frequencies of $k \cdot f_s \cdot L/(2M)$ where k is an integer. The reason is that on an average $L/2$ new DAC elements are

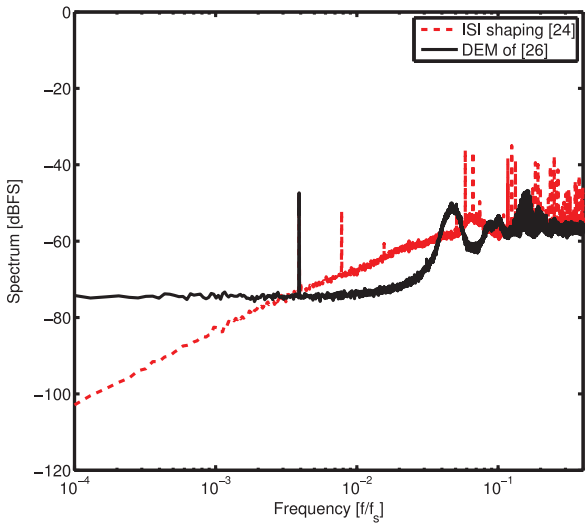

Fig. 15. Spectra of $\Gamma_i[n]$ for ISI shaping technique [24] and DEM of [26].

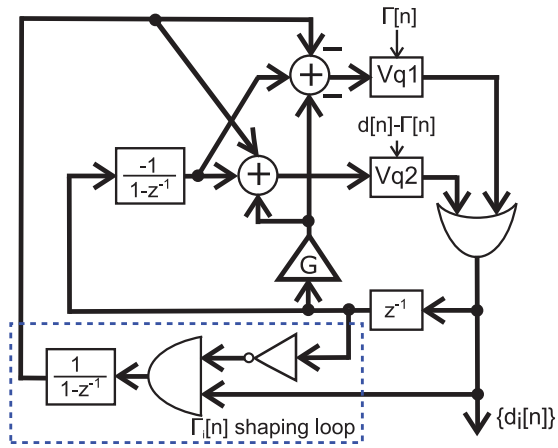

Fig. 16. Architecture of proposed DEM technique.

turned on every cycle. Since there are M elements in the DAC, each $d_i[n]$ takes on average $2M/L$ cycles to repeat its pattern. Since, $\Gamma_i[n] = (1 - d_i[n-1])d_i[n]$, each $\Gamma_i[n]$ also repeats every $2M/L$ cycles on average. This leads to noise peaks at $k \cdot f_s \cdot L/(2M)$.

Note that presence of noise peaks will increase in-band noise. Thus, there is a trade-off with respect to the choice of L. A higher value of L will increase the element switching rate and push the noise peaks away. This comes at the expense of reducing the range of $d[n]$ and degrading the redundancy available for ISI shaping. Note that this is similar to the trade-off in DWA which has the highest element switching rate, and hence, the best first-order static mismatch shaping, but also the worst ISI error.

E. Summary of Prior Works

Starting from the basic thermometer coding, researchers have proposed modified thermometer based RTC [19], RSTC [20] and the DEM of [21] which randomize the static mismatch. All these techniques achieve good ISI reduction by having very low DAC element switching similar to that in basic thermometer coding. The modified thermometer coding of [22] improves upon the existing thermometer-based techniques by achieving high-pass shaping of static mismatch while maintaining the same low element transition rate. All the thermometer based techniques rely on intrinsic quantization noise to achieve a better static mismatch reduction. Thus, these techniques are suitable for multi-bit, CT $\Delta\Sigma$ DACs with aggressive noise shaping. The thermometer based DEMs also show good decorrelation between $\Gamma[n]$ and the input $d[n]$. The MMS technique of [23] is an important leap forward and it showed that ensuring a constant transition density can turn a significant portion of the ISI error into offset, thus greatly improving DAC linearity. The ISI shaping technique of [24] achieves high-pass shaping of both static mismatch and ISI error and is a major advancement on the prior art. It also removes the limitations of requiring matched ISI errors of individual elements and equal ISI contribution from up and down transitions which the MMS algorithm suffers from. The work of [25] improves the ISI shaping performance by monitoring both up and down transitions instead of only the up transition as in [24]. However, both the ISI shaping techniques of [24], [25] show distortion at large amplitudes due to the dependence of instantaneous $\Gamma[n]$ on $d[n]$. The work of [26] addresses this limitation by ensuring that $\Gamma[n]$ is independent of $d[n]$ in every cycle while maintaining the high-pass shaping of $\Gamma[n]$. However, it still has a limitation similar to the MMS algorithm in that a reasonable matching between ISI errors of individual elements is expected. Thus, even though the technique of [26] can high-pass shape $\Gamma[n]$, it cannot high-pass shape $\Gamma_i[n]$. The technique of [26] and MMS algorithm have a restriction on the maximum value of $d[n]$ as discussed earlier, and is best suited for moderate out-of-band NTF gains. The ISI shaping techniques of [24], [25] can support a larger range of $d[n]$ at the cost of increased distortion at large values of $d[n]$. The modified thermometer coding techniques [19]–[22] do not have this restriction on the range of $d[n]$, but their static mismatch handling capability degrades if the out-of-band NTF gain is low.

IV. Proposed DEM With High-Pass Shaping of Mismatch and ISI Error of Individual DAC Elements

A. Proposed Technique

The limitation of not shaping $\Gamma_i[n]$ as in [26] can be solved by keeping track of the transition rates of each DAC element. This can be done by modifying the DEM in Fig. 13 as shown in Fig. 16.

The modification from the architecture in Fig. 13 are the two feedback loops that take into account the accumulation of up-transition rate for each DAC element. If any element in the DAC has made many up-transitions in previous cycles, the feedback loop will lower the priority for selection of the element by $Vq1$, and the feedback loop will increase the priority for selection of the element by $Vq2$. Thus, if an element in the

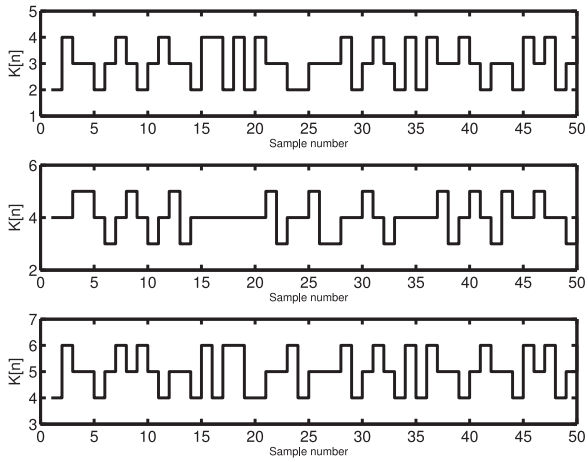

Fig. 17. $K[n]$ as a function of time for (a) $L = 3$ (b) $L = 4$ (c) $L = 5$.

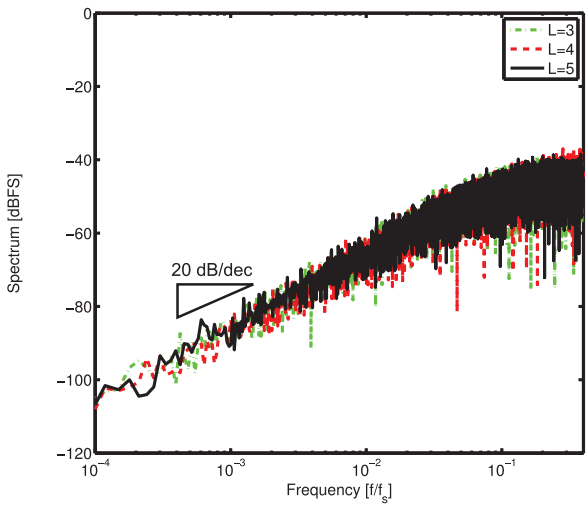

Fig. 18. Spectra of $K[n]$ for different L values.

DAC has a high accumulated $\Gamma_i[n]$, the proposed DEM tries to ensure that $d_i[n]$ does not make a transition in the next cycle. As a result, the long term average of $\Gamma_i[n]$ is identical for all elements leading to a high-pass shaped spectrum.

The element selection pattern every cycle is then decided in the following manner:

1) $\Gamma[n]$ unselected elements are turned on that have been least frequently used and have the lowest accumulated $\Gamma_i[n]$.
2) $(d[n] - \Gamma[n])$ selected elements are kept on that have been least frequently used and have the highest accumulated $\Gamma_i[n]$.

The total number of transitions, $K[n]$, as a function of time is shown in Fig. 17. It can be clearly seen that $K[n]$ varies between $L - 1$, L, and $L + 1$. The spectra of $K[n]$ for different L values are shown in Fig. 18. The first-order shaping of $K[n]$ can be clearly seen from Fig. 18. The absence of any tones in Fig. 18 show that $K[n]$ has good decorrelation with $d[n]$.

The spectra of $\Gamma_i[n]$ for the technique in [26] and the proposed DEM are shown in Fig. 19. A 32-element DAC, with an input of -3 dBFS was used for the simulation. A static mismatch error with a standard deviation of 1% and an ISI error with a mean of 1% and standard deviation of 1% was used. The first-order shaping of $\Gamma_i[n]$ for the proposed DEM can be clearly seen.

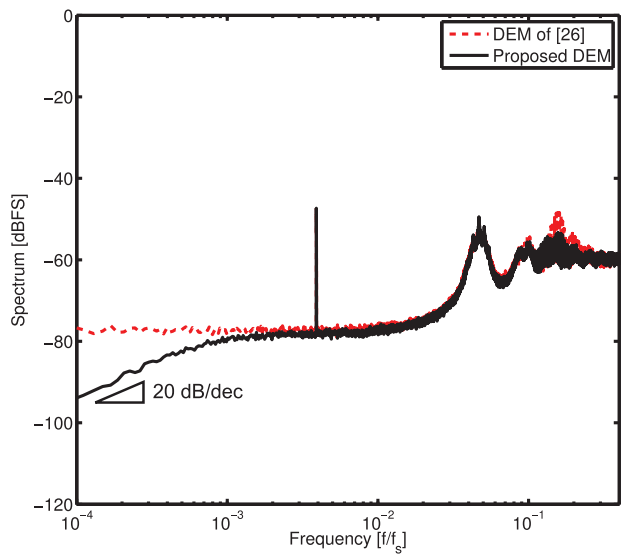

Fig. 19. Spectra of $\Gamma_i[n]$ for DEM of [26] and proposed DEM technique.

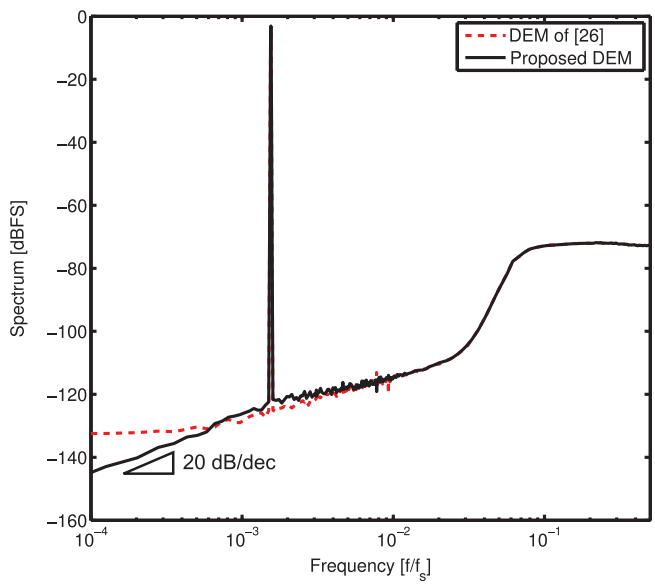

Fig. 20. Output spectra for DEM of [26] and the proposed DEM.

Fig. 20 shows the spectra of the DAC output for the technique of [26] and the proposed DEM. The same simulation conditions as for Fig. 19 were used. It can be clearly seen from Fig. 20 that the proposed DEM has a lower in-band noise and maintains in-band noise shaping even in the presence of mismatch between ISI errors in the DAC elements. These simulation results demonstrate that the proposed DEM can high-pass shape static mismatch and ISI error of each DAC element.

B. Hardware Complexity

Compared to the technique of [26], the proposed technique has an additional feedback loop with integrator and logic gates. This is a small increase in terms of hardware cost, specially for advanced technology nodes. The architecture of the proposed DEM has two vector quantizers. Each VQ has to perform a sorting of M elements which can be hardware intensive when M is large. As M increases, the hardware complexity increases

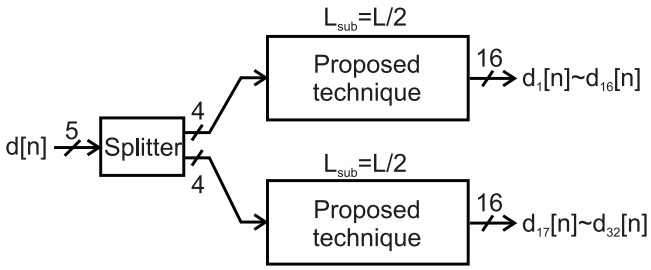

Fig. 21. Implementation of the proposed technique with reduced hardware complexity.

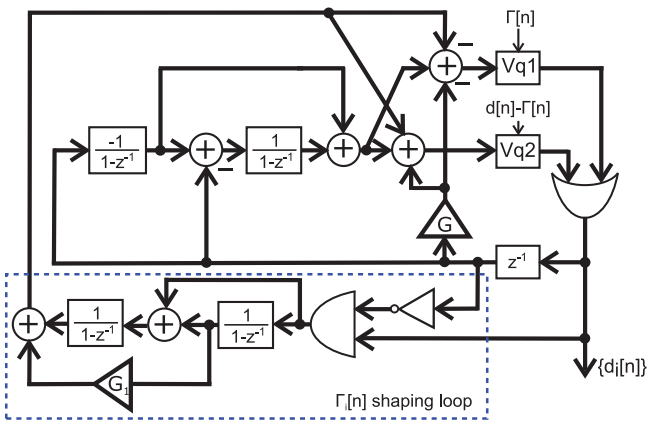

Fig. 22. Second-order mismatch and ISI shaping with the proposed DEM technique.

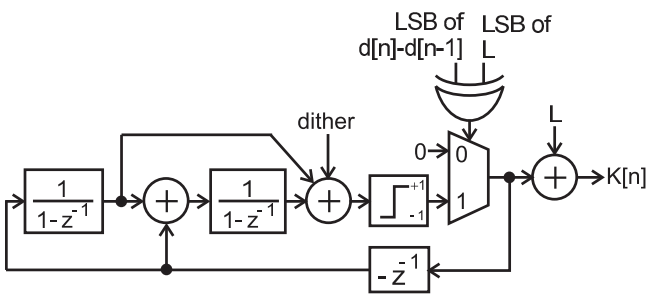

Fig. 23. Second-order shaped $K[n]$ generation technique.

in a super-linear fashion. To reduce the hardware complexity, the tree-structure of [9] can be adopted. Fig. 21 shows an example for $M = 32$. A splitter separates $d[n]$ into two 4-bit paths. Thus, two 4-bit sorters are needed instead of a 5-bit sorter which reduces the hardware complexity considerably. To use this splitting technique, each path has to ensure an average $L/2$ transitions to keep the overall number of transitions at L.

C. Second-Order $\Gamma_i[n]$ Shaping

The proposed technique can be extended to achieve higher order mismatch and ISI shaping. Fig. 22 shows the architecture for second-order mismatch and ISI shaping with the proposed technique. The filter used for second-order shaping of $\Gamma_i[n]$ is similar to the filter structure used in higher order VQ as shown in [10]. Fig. 23 shows the implementation of second-order high-pass shaped $K[n]$ generation block.

Fig. 24 shows second-order shaped $\Gamma_i[n]$ and $d_i[n]$ obtained using the architecture of Fig. 22. The second-order shaping can be clearly seen.

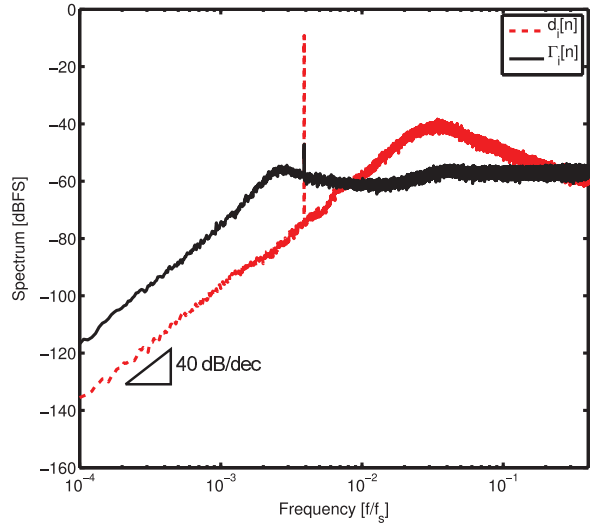

Fig. 24. Spectra of $\Gamma_i[n]$ and $d_i[n]$ for second-order mismatch and ISI shaping with the proposed DEM technique.

V. Simulation Results

To compare the proposed technique with the existing techniques, a 32-element, fifth-order $\Delta\Sigma$ DAC was used and 2^{17} point discrete-time simulation was performed. A maximum out-of-band NTF gain of 3 and input amplitude of -3 dBFS was used. The $\Delta\Sigma$ modulator is designed and optimized by using the MATLAB $\Delta\Sigma$ modulator toolbox [8]. An input signal frequency of $f_s/2664$ and OSR of 64 was used. The DAC elements are assumed to have a static mismatch with a zero mean and standard deviation of 1%. The ISI error is assumed to have a mean of 2% with a standard deviation of 1%. Thermal noise is added so that the thermal noise limited signal-to-noise ratio (SNR) at an OSR of 64 is 103.7 dB.

Fig. 25 shows the performance of the various DEM techniques. The basic thermometer coding minimizes the ISI error but shows a lot of harmonics due to static mismatch in the DAC elements and has an SNDR of 55.3 dB and SFDR of 60.7 dB. The random element selection technique whitens the static mismatch error, but cannot handle ISI error. As a result, its SNDR is reduced to 48.9 dB and the SFDR is 52.2 dB. DWA shapes the static mismatch error, but has a very large ISI error due to the increase in element switching rate. Thus, it shows a low SNDR of 41.2 dB and an SFDR of 44.5 dB. Second-order DEM has lower element switching rate than DWA, but its in-band noise is still dominated by ISI induced distortions. It has an SNDR of 48 dB and SFDR of 51.1 dB. The RSTC technique [20] whitens both the static mismatch and ISI error and has an SNDR of 53.7 dB and an SFDR of 76.2 dB which is better than pure thermometer coding. The modified thermometer technique of [22] minimizes the DAC element switching rate and also shapes the static mismatch error. However, at moderate values of out-of-band NTF gain, its static mismatch shaping performance is not as good as DWA. Thus, it has an SNDR of 64.4 dB and SFDR of 96 dB. The MMS technique [23] reduces the ISI induced distortion significantly and also shapes the static mismatch. It has an SNDR of 79.9 dB and an SFDR of 101.8 dB. The ISI shaping technique [24] high-pass shapes both static mismatch and ISI error. However, it shows a second-order distortion at -3 dBFS. Thus

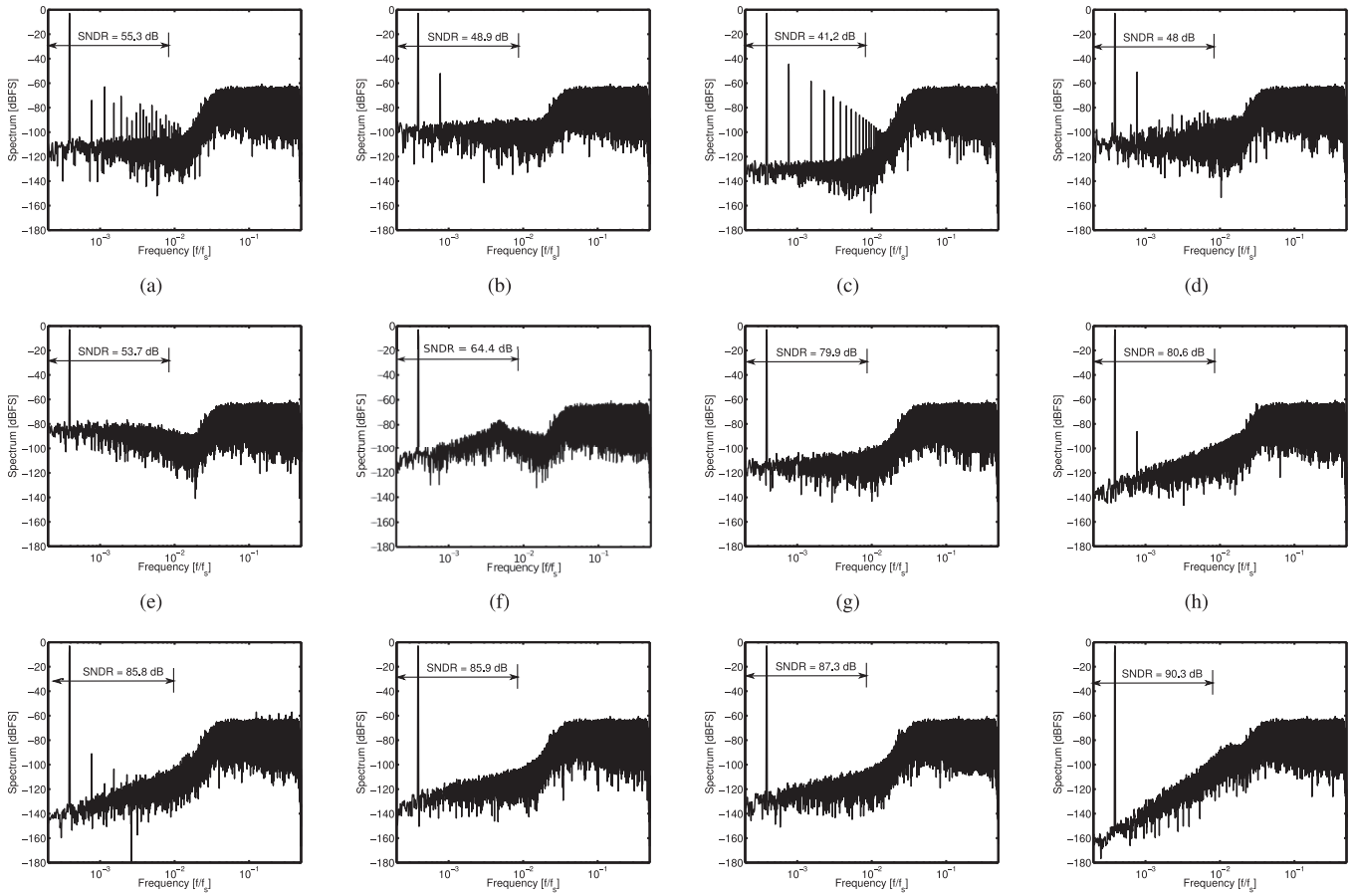

Fig. 25. DAC output spectra for (a) thermometer coding, (b) random selection, (c) DWA, (d) 2nd-order DEM, (e) RSTC [20], (f) modified thermometer coding [22], (g) MMS [23], (h) ISI shaping [24], (i) enhanced ISI shaping of [25], (j) DEM of [26], (k) proposed DEM with first-order shaping, and (l) proposed DEM with second-order shaping for -3 dBFS input.

it has an SNDR of 80.6 dB and SFDR of 86.4 dB. The enhanced ISI shaping technique of [25] monitors both up and down transitions and thus has a better ISI shaping performance than [24]. It has an SNDR of 85.8 dB and SFDR of 89.9 dB. The technique of [26] shapes both static mismatch and ISI error while maintaining good decorrelation between instantaneous transition rate and input. Thus it has an SNDR of 85.9 dB and a very good SFDR of $>$110 dB. The proposed DEM builds on the technique of [26] and removes its limitation of not shaping ISI error of individual elements. Thus, it has a better in-band noise than [26]. It has an SNDR of 87.3 dB and SFDR of $>$110 dB. The proposed DEM with second-order static mismatch and ISI shaping has an SNDR of 90.3 dB and SFDR of $>$120 dB. The simulation results are summarized in Table IV. It can be clearly seen that the proposed DEM maintains its superior performance over the existing art at both moderate and low OSR.

To compare the performance of the different ISI mitigation techniques, it is very important to look at their noise and distortion performance at different amplitudes. To this end, an input amplitude sweep was performed with the same simulation settings as used for Fig. 25. The SNR versus amplitude sweep plot is shown in Fig. 26. The proposed technique has the best SNR. The enhanced ISI shaping technique of [25] has a better SNR performance than the ISI shaping technique of [24] as it monitors both the up and down transitions thereby achieving finer resolution in transition rate count. The total-harmonic distortion (THD) versus input amplitude is shown in Fig. 27. The THD was computed by using the formula

$$\text{THD} = 10\log_{10}(\text{signal power}/\text{summation of power in harmonic bins}).$$

To get an accurate estimate of the power in the harmonics, a 2^{20} point simulation was performed with an averaging of 10 times. From Fig. 27, it can be seen that the proposed DEM has the best THD performance at large signal amplitudes. This is

TABLE IV
COMPARISON OF DIFFERENT DEM TECHNIQUES FOR MULTI-BIT $\Delta\Sigma$ DAC

	OSR=64		OSR=16	
	SNDR(dB)	SFDR(dB)	SNDR(dB)	SFDR(dB)
Ideal	103.7	$>$ 130	81.7	$>$ 130
Thermometer	55.3	60.7	55.1	60.7
Random selection	48.9	52.2	48.7	52.2
DWA	41.2	44.5	41.2	44.5
2nd-order DEM	48.0	51.1	47.9	51.1
Random swap [20]	53.7	76.2	51.3	76.2
DEM of [22]	64.4	96.0	51.5	81.7
MMS [23]	79.9	101.8	69.3	101.8
ISI shaping [24]	80.6	86.4	64.6	74.2
DEM of [25]	85.8	89.9	69.4	76.5
DEM of [26]	85.9	$>$ 110	71.4	$>$ 110
This work	87.3	$>$ 110	73.9	$>$ 110

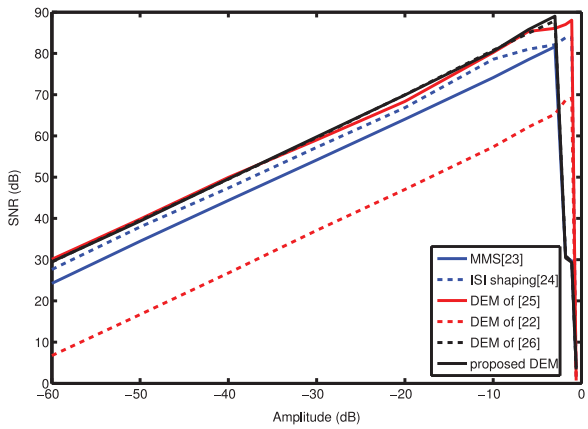

Fig. 26. Comparison of SNR versus amplitude for ISI reduction techniques.

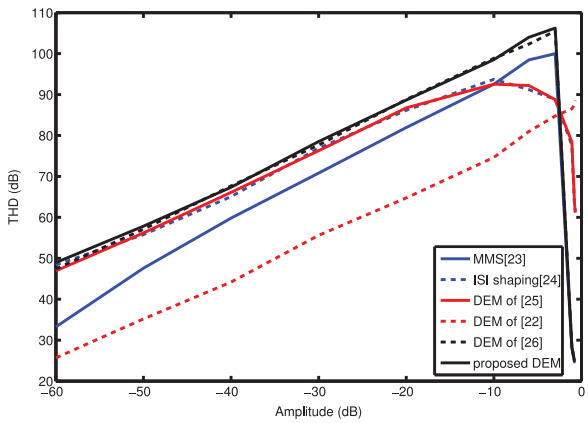

Fig. 27. Comparison of THD versus amplitude for ISI reduction techniques.

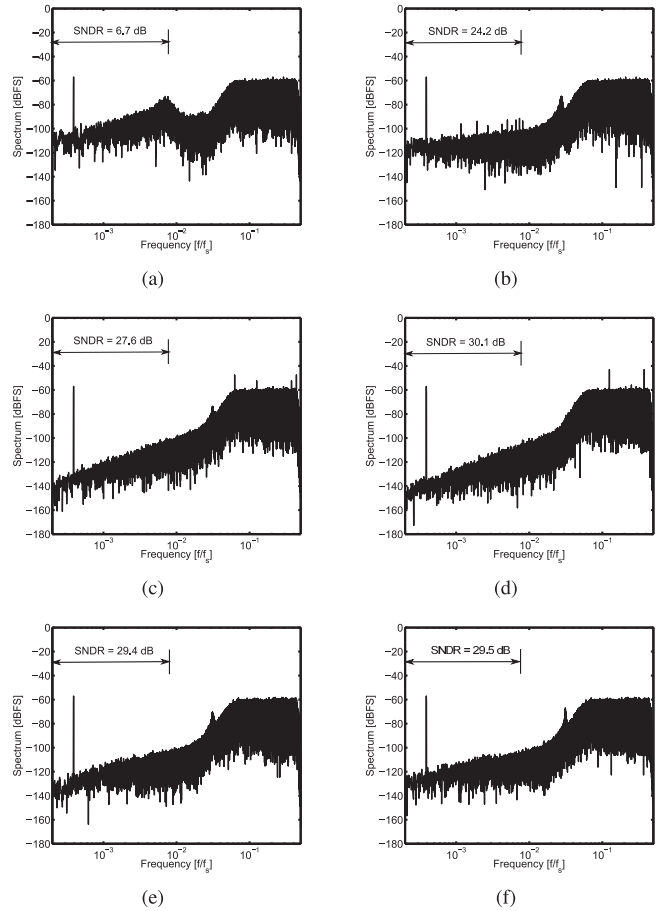

Fig. 28. DAC output spectra for (a) modified thermometer coding [22], (b) MMS [23], (c) ISI shaping [24], (d) enhanced ISI shaping of [25], (e) DEM of [26], and (f) proposed DEM with first-order shaping for −60 dBFS input.

due to the excellent decorrelation between instantaneous transition density and input achieved by the proposed DEM. The ISI shaping techniques of [24], [25] show degradation in THD performance above −6 dBFS due to increased correlation of instantaneous transition density with the input resulting in increased harmonic distortion. The MMS technique [23] performs better than the ISI shaping techniques of [24], [25] at large signal amplitudes due to better decorrelation between instantaneous transition density and input signal. At low signal amplitudes, the power in the harmonic bins is dominated by noise rather than distortion. For the proposed DEM as well as the DEM of [26], which have very low distortion, harmonic distortions go below the noise floor at input amplitudes smaller than −3 dBFS.

Finally, the output spectrum of different state-of-the-art ISI mitigation techniques at a small input amplitude of −60 dBFS is shown in Fig. 28. All the simulation conditions, except the input amplitude, are same as used for Fig. 25. It can be seen that at low signal amplitudes, the proposed DEM has no visible distortions and has a good SNDR of 29.5 dB. As is expected, at low input amplitudes, the enhanced ISI shaping technique [25] has the best SNDR due to its better ISI shaping performance as it keeps count of both up and down transitions rather than only one transition.

VI. Conclusion

Static mismatch is the main source of error in multi-bit DT $\Delta\Sigma$ modulators and most of the existing DEM algorithms are designed to address static mismatch. Recently, CT $\Delta\Sigma$ modulators have been more popular than DT $\Delta\Sigma$ modulators as CT $\Delta\Sigma$ modulators can operate at higher sampling frequency and/or consume less power. However in CT $\Delta\Sigma$ modulators, dynamic ISI error is a major concern. Most existing DEM techniques cannot handle ISI error as they increase element switching activity to high-pass static mismatch. This paper has presented a novel technique to simultaneously high-pass shape static mismatch and ISI error of each DAC element in a multi-bit, CT $\Delta\Sigma$ modulator. The proposed technique also ensures a good decorrelation of the instantaneous transition density from the input signal. Existing works on ISI reduction has been reviewed and the proposed technique is compared with existing art. The proposed DEM is purely digital in nature and is expected to be useful for high performance, CT $\Delta\Sigma$ modulators.

Acknowledgment

The authors thank Dr. R. Hezar and Dr. L. Risbo for insightful discussions and Dr. R. Schreier for sharing the MATLAB $\Delta\Sigma$ modulator toolbox.

REFERENCES

[1] U.-K. Moon, J. Silva, J. Steensgaard, and G. C. Temes, "Switched-capacitor DAC with analogue mismatch correction," *Electron. Lett.*, vol. 35, no. 22, pp. 1903–1904, 1999.

[2] R. T. Baird and T. S. Fiez, "A low oversampling ratio 14-b 500-khz ADC with a self-calibrated multibit DAC," *IEEE J. Solid-State Circuits*, vol. 31, no. 3, pp. 312–320, Mar. 1996.

[3] M. De Bock, X. Xing, L. Weyten, G. Gielen, and P. Rombouts, "Calibration of DAC mismatch errors in ADCs based on a sine-wave measurement," *IEEE Trans. Circuits Syst. II, Exp. Briefs*, vol. 60, no. 9, pp. 567–571, Sep. 2013.

[4] R. J. Van De Plassche, "Dynamic element matching for high-accuracy monolithic D/A converters," *IEEE J. Solid-State Circuits*, vol. 11, no. 6, pp. 795–800, Dec. 1976.

[5] H. S. Jackson, "Circuit and method for cancelling nonlinearity error associated with component value mismatches in a data converter," U.S. Patent 5 221 926, Jun. 1993.

[6] R. T. Baird and T. S. Fiez, "Linearity enhancement of multibit $\Delta\Sigma$ A/D and D/A converters using data weighted averaging," *IEEE Trans. Circuits Syst. II, Analog Digital Signal Process.*, vol. 42, no. 12, pp. 753–762, Dec. 1995.

[7] K.-D. Chen and T.-H. Kuo, "An improved technique for reducing baseband tones in sigma-delta modulators employing data weighted averaging algorithm without adding dither," *IEEE Trans. Circuits Syst. II, Analog Digital Signal Process.*, vol. 46, no. 1, pp. 63–68, Jan. 1999.

[8] R. Schreier and B. Zhang, "Noise-shaped multbit D/A convertor employing unit elements," *Electron. Lett.*, vol. 31, no. 20, pp. 1712–1713, 1995.

[9] I. Galton, "Spectral shaping of circuit errors in digital-to-analog converters," *IEEE Trans. Circuits Syst. II, Analog Digital Signal Process.*, vol. 44, no. 10, pp. 808–817, Oct. 1997.

[10] N. Sun, "High-order mismatch-shaping in multibit DACs," *IEEE Trans. Circuits Syst. II, Exp. Briefs*, vol. 58, no. 6, pp. 346–350, Jun. 2011.

[11] N. Sun and P. Cao, "Low-complexity high-order vector-based mismatch shaping in multibit $\Delta\Sigma$ ADCs," *IEEE Trans. Circuits Syst. II*, vol. 58, no. 12, pp. 872–876, Dec. 2011.

[12] N. Sun, "High-order mismatch-shaped segmented multibit $\Delta\Sigma$ DACs with arbitrary unit weights," *IEEE Trans. Circuits Syst. I, Reg. Papers*, vol. 59, no. 2, p. 295, Feb. 2012.

[13] T. Shui, R. Schreier, and F. Hudson, "Mismatch-shaping DAC for low-pass and bandpass multi-bit delta-sigma modulators," in *Proc. 1998 IEEE Int. Symp. Circuits Syst.*, 1998, vol. 1, pp. 352–355.

[14] Q. Mu, J. O. Coleman, D. P. Scholnik, and Z. Popovic, "Circuit approaches to nonlinear-ISI mitigation in noise-shaped bandpass D/A conversion," *IEEE Trans. Circuits Syst. I, Reg. Papers*, vol. 57, no. 7, pp. 1559–1572, Jul. 2010.

[15] J. G. Kauffman, R. Ritter, C. Chu, and M. Ortmanns, "A DAC cell with improved ISI and noise performance using native switching for multi-bit CT Delta Sigma modulators," in *Proc. 2013 IEEE Int. Symp. Circuits Syst.*, 2013, pp. 574–577.

[16] T. Doorn *et al.*, "An audio FIR-DAC in a BCD process for high power class-D amplifiers," in *Proc. 31st IEEE Eur. Solid-State Circuits Conf.*, 2005, pp. 459–462.

[17] T. Rueger *et al.*, "A 110 dB ternary PWM current-mode audio DAC with monolithic 2 Vrms driver," in *IEEE Int. Solid-State Circuits Conf. Dig. Tech. Papers*, 2004, pp. 372–533.

[18] R. Hezar, L. Risbo, H. Kiper, M. Fares, B. Haroun, G. Burra, and G. Gomez, "A 110 dB SNR and 0.5 mW current-steering audio DAC implemented in 45 nm CMOS," in *IEEE Int. Solid-State Circuits Conf. Dig. Tech. Papers*, Feb. 2010, pp. 304–305.

[19] D.-H. Lee, T.-H. Kuo, and K.-L. Wen, "Low-cost 14-bit current-steering DAC with a randomized thermometer-coding method," *IEEE Trans. Circuits Syst. II, Exp. Briefs*, vol. 56, no. 2, pp. 137–141, Feb. 2009.

[20] M.-H. Shen, J.-H. Tsai, and P.-C. Huang, "Random swapping dynamic element matching technique for glitch energy minimization in current-steering DAC," *IEEE Trans. Circuits Syst. II, Exp. Briefs*, vol. 57, no. 5, pp. 369–373, May 2010.

[21] P. Wang and N. Sun, "A random DEM technique with minimal element transition rate for high-speed DACs," in *Proc. 2014 IEEE Int. Symp. Circuits Syst.*, 2014, pp. 1155–1158.

[22] A. Sanyal, P. Wang, and N. Sun, "A thermometer-like mismatch shaping technique with minimum element transition activity for multi-bit $\Delta\Sigma$ DACs," *IEEE Trans. Circuits Syst. II, Exp. Briefs*, vol. 61, no. 7, pp. 461–465, Jul. 2014.

[23] T. Shui, R. Schreier, and F. Hudson, "Mismatch shaping for a current-mode multibit delta-sigma DAC," *IEEE J. Solid-State Circuits*, vol. 34, no. 3, pp. 331–338, Mar. 1999.

[24] L. Risbo, R. Hezar, B. Kelleci, H. Kiper, and M. Fares, "Digital approaches to ISI-mitigation in high-resolution oversampled multi-level D/A converters," *IEEE J. Solid-State Circuits*, vol. 46, no. 12, pp. 2892–2903, Dec. 2011.

[25] A. Sanyal and N. Sun, "An enhanced ISI shaping technique for multi-bit $\Delta\Sigma$ DACs," in *Proc. 2014 IEEE Int. Symp. Circuits Syst.*, 2014, pp. 2341–2344.

[26] A. Sanyal, L. Chen, and N. Sun, "Dynamic element matching with signal-independent element transition rates for multibit $\Delta\Sigma$ modulators," *IEEE Trans. Circuits Syst. I,*, vol. 62, no. 5, pp. 1325–1334, May 2015.

[27] A. Sanyal and N. Sun, "A simple and efficient dithering method for vector quantizer based mismatch-shaped $\Delta\Sigma$ DACs," in *Proc. IEEE Int. Symp. Circuits Syst.*, 2012, pp. 528–531.

Arindam Sanyal (S'14) received the M.Tech. degree from the Indian Institute of Technology, Kharagpur, India, in 2009. He is a Ph.D. degree student in the integrated circuits and systems track at the University of Texas at Austin, Austin, TX, USA.

He is currently working as a Design Engineer in Silicon Laboratories, Austin, TX, USA. He has worked as a Graduate Research intern at Intel Austin and at Silicon Laboratories, Austin. His current research interests are VCO-based ADC design and error correction in multi-bit $\Delta\Sigma$ DACs.

Nan Sun (M'11) received the B.S. degree from Tsinghua University, Beijing, China, in 2006, where he ranked top in the Electrical Engineering Department and graduated with the highest honor, and the Ph.D. degree from Harvard University, Cambridge, MA, USA, in 2010.

He is an Assistant Professor at the University of Texas at Austin, Austin, TX, USA. His research interests include: analog, mixed-signal, and RF integrated circuits; miniature spin resonance systems; low-cost medical imaging systems; sensors and actuators.

Dr. Sun received the first-class Outstanding Student Award from Tsinghua University each year from 2003 to 2006. He won the Top Prize in the Intercollegiate Physics Competition in 2003. He is the recipient of Samsung Fellowship, Hewlett Packard Fellowship, and Analog Devices Outstanding Student Designer Award in 2003, 2006, and 2007, respectively. He also won the Harvard Teaching Award in three consecutive years: 2008, 2009, and 2010. He received the NSF Early Career Award in 2013. He currently serves as the Technical Program Chair of ASSCC and as the guest editor for IEEE Internet of Things Journal.